Ab initio study of anthracene under high pressure

Kerstin Hummer,* Peter Puschnig, and Claudia Ambrosch-Draxl
Institut für Theoretische Physik, Karl-Franzens Universität Graz, Universitätsplatz 5, A-8010 Graz, Austria
(Received 5 June 2002; revised manuscript received 12 March 2003; published 7 May 2003)

The pressure effect on the internal molecular orientation, the electronic and optical properties of crystalline anthracene is calculated up to 10.2 GPa by performing density-functional calculations. As the only input for our *ab initio* calculations we use the lattice parameters experimentally determined by x-ray powder diffraction under pressure and optimize the internal geometry with respect to the three angles θ, χ, and δ, which define the orientation of the molecules inside the unit cell. For the optimized structures the isothermal bulk moduli, the electronic band structures, and dielectric tensors as a function of the unit-cell volume are calculated. The structure optimizations using the local-density approximation and the generalized gradient approximation exchange-correlation potentials give very similar results and agree well with the internal geometry determined from experiment. This gives rise to the conclusion that the application of such approximations for the description of organic molecular crystals within density-functional theory is valid. Moreover, the electron distribution clearly shows a finite density between the molecules in the unit cell, which increases with pressure due to the enhancement of the intermolecular interactions. These findings support the interpretation that the bonding mechanism in anthracene is not solely van der Waals interaction.

DOI: 10.1103/PhysRevB.67.184105 PACS number(s): 61.50.Ah, 71.15.Nc, 71.20.Rv, 78.40.Me

I. INTRODUCTION

Since the discovery of electrical conductivity in doped polyacetylene,[1,2] organic polymers are of great scientific and technological interest.[3,4] Considerable attention has also been paid to semiconducting materials consisting of small organic molecules, such as oligophenylens, oligothiophenes, and linear oligoacenes. Exhibiting photoconductivity and electroluminescence[5–8] these are promising materials for optoelectronic devices. Up to now a large number of experimental investigations concerning the characteristics of devices based on linear oligoacenes or oligothiophenes, e.g., quantum or conversion efficiencies and the charge-carrier mobilities, have been performed.[10,6,9] For the origin of the latter, two possible approaches, the *hopping model* and the *band model* have been discussed in literature.[11] Experimental studies of the charge transport in single-crystal naphthalene as a function of temperature suggested that the transport mechanism changes from coherent bandlike at low temperature to incoherent hopping type at high temperatures.[12] In a more recent work, high carrier mobilities have been found for anthracene[9] making this material a good candidate for applications.

The physical properties strongly depend on the crystalline structure of such materials, which in turn is governed by the intermolecular interactions in the solid state. Their relation to the electronic and optical properties is essential for device design and efficient applications. Once their role is clarified, one will gain insight in the material-dependent electro-optical activity, but also a deeper understanding of the charge-transport properties. One possibility to alter the intermolecular interactions in a controlled way is to apply hydrostatic pressure. By the reduction of the unit-cell volume the overlap of the molecular orbitals is enhanced giving rise to stronger intermolecular interaction. In this work, we study the pressure effect on the structural, electronic, and optical properties of anthracene as a representative for oligoacenes by *ab initio* calculations based on density-functional theory (DFT). The results should help to validate this procedure for such molecular crystals, which are generally believed to be van der Waals bound. In our calculations we use the local-density approximation (LDA) and the generalized gradient apprioximation (GGA) for the exchange-correlation (xc) functionals, both of which do not include long-range van der Waals (vdW) interactions. Therefore the comparison of our theoretical findings with experimental results should prove the applicability of different xc functionals for calculating structural properties of organic molecular crystals. We optimize the internal geometry of anthracene as a function of pressure and investigate the effect of the intermolecular and interchain interactions. For the optimized structures we obtain the bulk modulus as a function of volume, and further, the pressure dependence of the electronic band structure, the energy gap, and the dielectric tensor.

II. METHODS OF CALCULATION

A. Internal geometry optimization

At room temperature and ambient pressure anthracene, $C_{14}H_{10}$, crystallizes in the monoclinic space group $P2_1/a$, which is characterized by the lattice parameters $a=8.562$Å, $b=6.038$ Å, $c=11.184$ Å, and $\beta=124.7°$.[13] In Fig. 1 two projections of the crystal structure are shown to illustrate two features, which are common for many organic molecular crystals. One is the *herringbone* stacking of the two inequivalent planar rodlike molecules (top left) and the second is the layered structure in the crystalline c direction (bottom left). A single anthracene molecule consists of sp^2-hybridized carbon atoms. Each carbon forms three covalent σ bonds, the fourth valence electron stays in a $2p$ orbital perpendicular to the molecular plane generating the π-electron cloud. For this reason the intramolecular bonds are rather rigid and displacements of the carbon atoms result in big atomic forces. In contrast, rotations of the rigid molecule are accompanied by much smaller total energy

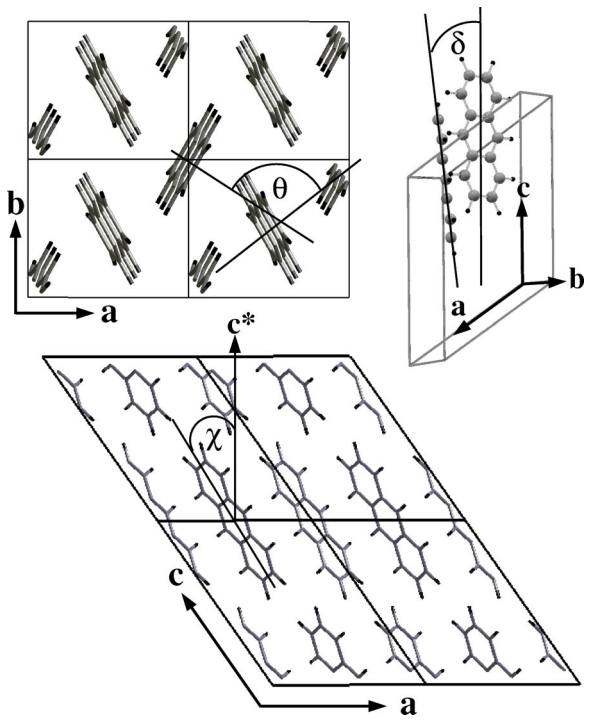

FIG. 1. The projections of the crystal structure on the (ab) plane (top left) and the (ac) plane (bottom left) illustrate the herringbone stacking and the layered structure, respectively. In addition, the three angles θ, χ, and δ, which served as the parameters for the geometry optimization, are defined.

changes. Therefore the most effective procedure in theoretically determining the internal geometry turned out to consist of two steps. At the beginning, we optimized the internal molecular geometry by minimizing the forces acting on the atoms to be below 1 mRy/a.u. Subsequently, we minimized the total energy with respect to the orientation defined by the angles θ, χ, and δ (see Fig. 1). The herringbone angle θ quantifies the angle between the normal vectors of the molecular planes of two translationally inequivalent molecules. The tilting angle of the long molecular axis with respect to the c^* axis [perpendicular to the (ab) plane] is denoted by χ. The angle between the long molecular axes of two translationally inequivalent molecules is labeled δ. Thus the variation of these angles corresponds to rotations of the rigid molecules. We optimized the herringbone angle θ at fixed χ and δ first. Then we kept the optimized θ and successively varied χ and δ. The internal geometry optimization was finished with a final relaxation of the atomic positions such that the atomic forces were less than 1 mRy/a.u.

B. Computational details

Starting from the experimentally determined lattice parameters as a function of pressure (see Table I) we performed *ab initio* calculations using the full-potential linearized augmented plane wave (FP-LAPW) formalism as implemented in the WIEN97 code.[14] In particular, the APW+lo (local orbitals) extension[16] to the WIEN97 package was used. Compared to the conventional LAPW method, the APW+lo method permits us to decrease the plane-wave cutoff $R_{MT}K_{max}$. Thus the size of the Hamilton matrix, and therefore the computational effort, is considerably reduced. Exchange and correlation effects are treated by LDA (Ref. 17) and GGA.[18] Throughout the paper LDA results are shown, whereas the GGA data are used for comparison to be analyzed in the discussion section.

TABLE I. Monoclinic lattice parameters a,b,c,β, and the unit-cell volume $V=a\cdot b\cdot c\cdot \sin\beta$ of anthracene as a function of pressure p.

p [GPa]	a [Å]	b [Å]	c [Å]	β [deg]	V [Å^3]
0.0[a]	8.510	6.027	11.162	124.63	475.35
1.1[b]	8.117	5.850	10.886	125.29	421.94
2.5[b]	7.893	5.753	10.759	125.75	396.50
3.1[b]	7.828	5.724	10.724	125.87	389.32
4.0[b]	7.733	5.679	10.669	126.02	378.96
6.1[b]	7.572	5.601	10.592	126.48	361.23
8.0[b]	7.444	5.533	10.517	126.81	346.85
10.2[b]	7.347	5.483	10.470	127.07	336.55

[a]From Ref. 13.
[b]From Ref. 15.

The following input parameters have been kept constant throughout all calculations: In order to avoid atomic sphere overlap at higher pressures we fixed the muffin tin radii to 1.28 a.u. for carbon atoms (C) and to 0.75 a.u. for hydrogen atoms (H). A $R_{MT}K_{max}$ of 3.0 Ry for H (i.e., 5.12 Ry for C), resulting in approximately 3000 plane waves, turned out to be sufficient for the accurate calculation of the atomic forces and the total energy within the APW+lo method. In the case of the internal structure optimization we used six $\boldsymbol{k}$ points in the irreducible Brillouin zone (IBZ) for the $\boldsymbol{k}$-space integrations by the improved tetrahedron method.[19] The atomic forces were converged better than 1 mRy/a.u. resulting in a total energy convergence of 0.1 mRy. The band structure calculations have been carried out following a path along Y, Γ, K, Z, B, and A. The internal coordinates of these points are (0.5,0,0), (0,0,0), (0.4,0,0.2), (0,0,0.5), (0,0.5,0), and (0.5,0.5,0) in units of $(2\pi/a,2\pi/b,2\pi/c)$, respectively. Note that $\overline{\Gamma Y}$ ($\overline{\Gamma B}$) is parallel to the crystalline a axis (b axis), and $\overline{\Gamma Z}$ corresponds to the c direction, which is approximately the long molecular axis. The momentum matrix elements that provide the selection rules for the frequency-dependent complex dielectric tensor have been computed on a dense grid of 413 irreducible $\boldsymbol{k}$ points in an energy window from plus to minus 1.5 Ry with respect to the Fermi level. The dielectric function has been calculated in the long-wavelength limit within the random-phase approximation.[20] In order to account for the self-energy correction, a $\boldsymbol{k}$-independent rigid upward shift of the conduction bands[21,22] Δ_c of 1.9 eV has been included. A lifetime broadening of 0.1 eV was applied in order to obtain smooth optical spectra.

III. RESULTS

A. Internal geometry

The results of the internal structure optimization are plotted in Fig. 2, where the calculated quantities θ, χ, and δ as

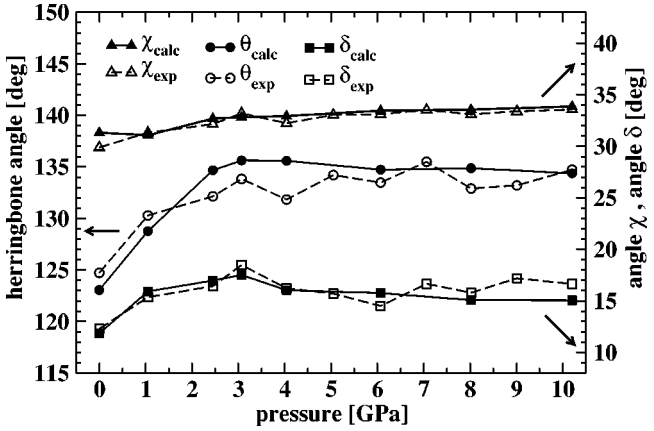

FIG. 2. FP-APW+lo results (full lines with filled symbols): the angles θ, χ, and δ are compared to the values refined from experiment (dashed lines with open symbols) as a function of pressure.

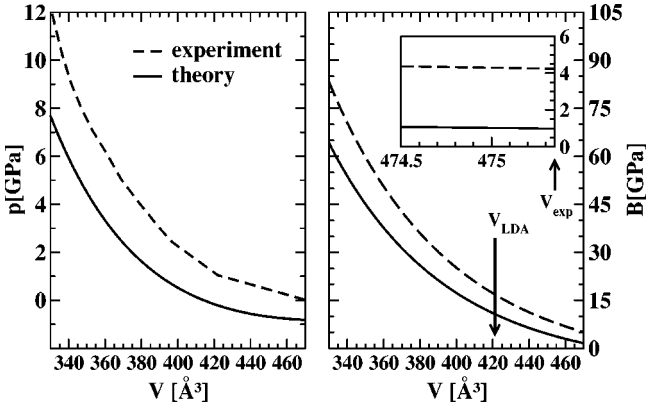

FIG. 3. The pressure as a function of volume calculated by a fit [Eq. (1)] of the theoretical data set (full line) and the experimental data set (dashed line) is shown in the left panel. In the right panel the isothermal bulk modulus versus volume for these two data sets resulting from the fit function is plotted. In the inset we focus on the region at the true equilibrium volume (V_{exp}=475.35 Å^3). V_{LDA} marks the LDA equilibrium volume.

a function of pressure are compared to the experimentally determined values. In good agreement with experiment all three angles increase over the pressure region from 0 to 10.2 GPa. The increase of θ, i.e., aligning the translationally inequivalent molecules, is the dominating effect. It is largest in the pressure range from 0 to 3 GPa, where θ raises by 12.6° and then slightly drops off up to 10.2 GPa. δ has a similar trend, but exhibits changes smaller in magnitude (i.e., +5.7° between 0 and 3 GPa). In contrast, χ increases by only 2.5° up to a pressure of 10.2 GPa. It can be argued that the behavior of χ and δ is due to the reduction of the lattice parameter c and the associated decrease of the layer distance, while the variation of θ is caused by the decrease of the lattice parameter a.[15] The largest change of a can be traced back to the highest linear compressibility in the a direction.[23] The argument that interchain interactions are responsible for the pressure effect on δ was proven by total-energy calculations for unit cells with elongated c axes. Starting from the crystal structure at ambient pressure we increased c by 1 (2) Å and varied the angle δ between 6° and 18°. The stretching of the c-axis raises the HH-distance, i.e., the shortest distance between end-hydrogen atoms of neighboring molecules in the c direction, from 2.4 to 3.4 (4.4) Å, respectively. Up to an HH distance of approximately 4 Å the interchain interaction is important and a total-energy minimum is found for δ=12°. For larger layer distances the energy changes become smaller and no global energy minimum exists in the considered range.

Comparing the pressure effects on the shortest intermolecular distances and on the bond lengths we confirm the expected result that the intramolecular interactions (covalent σ and π bonds inside the molecules) are less sensitive to pressure than the intermolecular interactions. The decrease in CC-bond and CH-bond lengths turned out to be 1–15 mÅ between 0 and 10 GPa. In contrast, the shortest intermolecular CH and HH distances reduce by several hundreds of mÅ, i.e., 630 and 420 mÅ, respectively.

To analyze how sensitively the three internal structure parameters θ, χ, and δ depend on the approximation for the xc potential, the internal structure optimization up to 4 GPa has been carried out using LDA and GGA. The GGA results turned out to be very similar to the LDA findings. GGA also yields an overall increase of the three angles as a function of pressure and the trend obtained with LDA is fully reproduced.

B. Isothermal bulk modulus

Birch[24] derived an equation of state (EOS) for calculating the isothermal bulk modulus from the total energy E as a function of volume V:

$$E(V)=E_0+\frac{9}{8}B_0V_0\left[\left(\frac{V_0}{V}\right)^{2/3}-1\right]^2+\frac{9}{16}B_0V_0(B_0'-4)\times\left[\left(\frac{V_0}{V}\right)^{2/3}-1\right]^3-\sum_{n=1}^{N}\gamma_n\left[\left(\frac{V_0}{V}\right)^{2/3}-1\right]^n, \qquad (1)$$

where B_0 and V_0 denote the isothermal bulk modulus and the equilibrium volume at ambient pressure, respectively. B_0' and γ_n are the first- and higher-order derivatives of B_0. Starting from LDA total energies E versus unit-cell volume V we calculated B_0 and the first derivative B_0' using the Birch EOS up to the power of 3. Applying the same fit to the experimental data set we calculated the experimental counterparts for comparison by making use of the relation $p=-\partial E/\partial V$. The volume dependence of the isothermal bulk modulus is then obtained from the fitted function. Figure 3 summarizes the results of this analysis. In the left panel the theoretical and the experimental pressure data as a function of volume are compared. The theoretical curve is shifted with respect to the experimental one, but the pressure dependence of the volume is reproduced. In the right panel of Fig. 3 the bulk modulus as a function of volume is depicted, which exhibits an analogous trend as $p(V)$. B_0 (B_0') calculated at the true equilibrium volume V_{exp} using the theoretical and experimental fit functions at ambient pressure are 0.98 GPa (9.66) and 4.24 GPa (15.97), respectively (inset of right panel in

Fig. 3). In contrast, the theoretical B_0 evaluated at the LDA (GGA) equilibrium volume V_0^{LDA} (V_0^{GGA}) is 12.61 (15.98) GPa. Using different types of EOS for fitting the experimental data B_0 values between 5.34 and 11.49 GPa have been obtained.[25,26] All these discrepancies reflect the fact that such organic materials are soft (related to small energy differences upon modification) and make clear that different EOS as well as the usage of different xc potentials can only reproduce the order of magnitude, but not an unambiguous value for the bulk modulus.

C. Band structure and DOS

The main features of the band structure of anthracene are anisotropic band dispersion and band splitting, which are three-dimensional (3D) effects and originate from the overlap of the π-wave functions of neighboring molecules. Both are a measure for the intermolecular interactions. Particularly, band splitting is due to the two translationally inequivalent molecules per unit cell and causes the *Davydov doublets* present in the excitation spectra of anthracene.[27] Since it has been found that the intermolecular distances are reduced and thus the intermolecular interactions are enhanced with increasing pressure, we expect both, band splitting and band dispersion to increase accompanied by a broadening of the density of states. These effects are apparent in the band structure and total density of states (DOS) presented in Fig. 4. As a matter of symmetry the bands are degenerate at *Y*, *B*, i.e., the zone boundaries of the IBZ in the *a* and *b* direction, respectively, and along $\overline{BA}$. This finding is in agreement with earlier calculations performed by Katz *et al.*[28] and by Silbey *et al.*[29,30] While upon pressure the symmetry and thus the degeneracy of the bands in this parts of the band structure is not changed, the band splitting becomes large at the zone center, along $\overline{\Gamma Z}$, and $\overline{KZ}$. However, the intermolecular interactions are anisotropically altered with pressure due to the nonuniform pressure dependence of the lattice parameters.[15] Therefore the increase in bandwidths and band splitting is strongly direction dependent. In the following we abbreviate the valence (conduction) -band pair with VB (CB) and a subscript, which denotes the sequence of the single bands within this pair downwards (upwards) in energy from the Fermi level. Both, VB and CB exhibit maximum band splitting at the *Z* point, which is 0.30 and 0.49 eV, respectively. The band splitting increases upon pressure, e.g., at 10.2 GPa it is 0.6 (1.36) eV for VB (CB) at *Z*. This is true for the whole band structure, except for VB at Γ, where VB_1 and VB_2 are almost degenerate at 10.2 GPa.

Figure 5 shows the bandwidths of CB_1, VB_1, and VB_2 evaluated in the directions $\overline{\Gamma Y}$, $\overline{\Gamma B}$, $\overline{\Gamma Z}$, and $\overline{\Gamma K}$ for the investigated pressure region. The increase of the bandwidths with pressure is largest along $\overline{\Gamma Y}$ for all bands. This is in accordance with the pressure dependence of the lattice parameter *a*, which is affected most by pressure.[15] The maximum gain in bandwidth for VB_1 and CB_1 with pressure is 0.28 and 0.46 eV, respectively. At ambient pressure the band dispersion of CB_1 is highest in $\overline{\Gamma Y}$, which is perpendicular to the long molecular axis and parallel to the herringbone-stacking direction. Since the charge-carrier mobility is inversely dependent on the effective mass and thus proportional to the bandwidth, the electron carrier mobility is largest in the crystalline *a* axis. This remains unchanged up to high pressures. In contrast to the electron conduction at ambient pressure, theory suggests $\overline{\Gamma B}$ and $\overline{\Gamma Z}$ as the favored channels for hole carriers. However, with increasing pressure the gain in bandwidth of VB_1 becomes more pronounced along $\overline{\Gamma Z}$ and thus the hole conduction is supposed to be largest in direction of the long molecular axis from approximately 3 GPa on. Comprising these results we can conclude that the pressure effect on the bandwidths is opposite to that caused by raising temperature, which localizes the charge

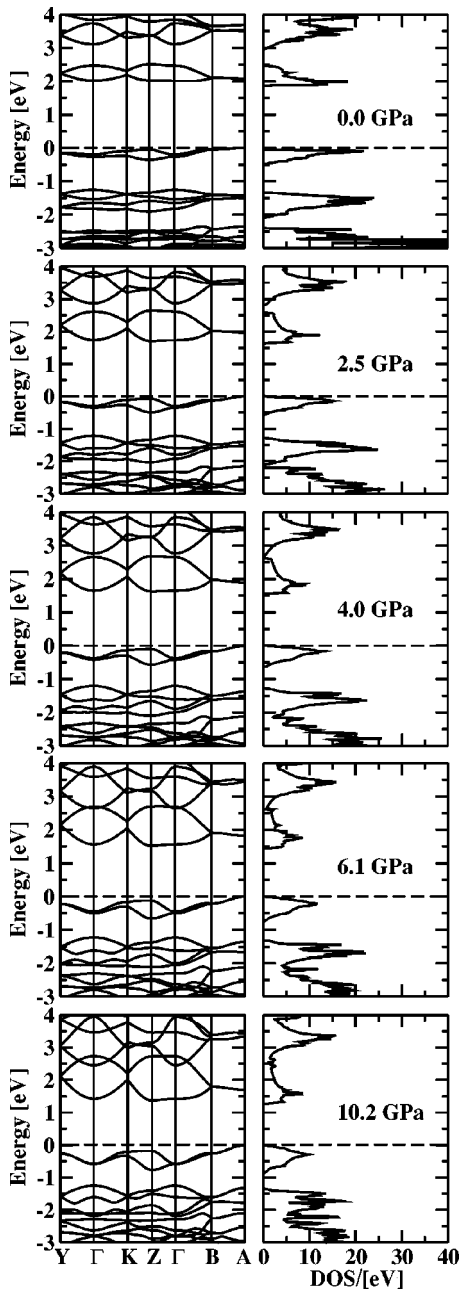

FIG. 4. Band structure $E(\boldsymbol{k})$ (left) and DOS (right) of anthracene at ambient pressure, 2.5, 4.0, 6.1, and 10.2 GPa, respectively. In each case the Fermi level is indicated by a dashed line.

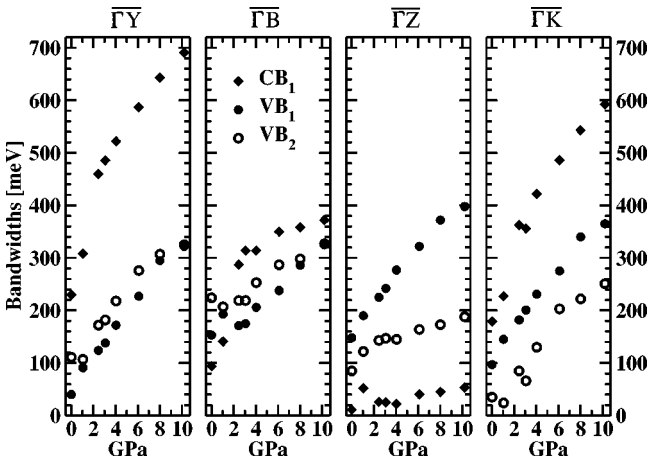

FIG. 5. Bandwidths of CB_1, VB_1, and VB_2 evaluated in the directions $\overline{\Gamma Y}$, $\overline{\Gamma B}$, $\overline{\Gamma Z}$, and $\overline{\Gamma K}$ as a function of pressure.

carriers in well confined bands with small bandwidths resulting in large effective charge-carrier masses. In order to gain insight into the origin of the different band dispersion and band splitting properties we calculate the electron densities, which are discussed in the following section.

D. Electron densities

The previously presented band structures revealed a very anisotropic pressure effect on the bands close to the Fermi level, e.g., on VB_1 and VB_2 along $\overline{\Gamma KZ}$. In this section, we have a closer look at the spatial variation of the contributions to the electron density calculated for CB_1, VB_1, and VB_2 as a sum over 40 $\boldsymbol{k}$ points along $\overline{\Gamma KZ}$ at different pressure values. The results obtained for the (ab) plane at different z coordinates are plotted in Figs. 6 and 7 for ambient pressure and 10.2 GPa, respectively. These density distributions evidence the enhancement of the intermolecular interactions

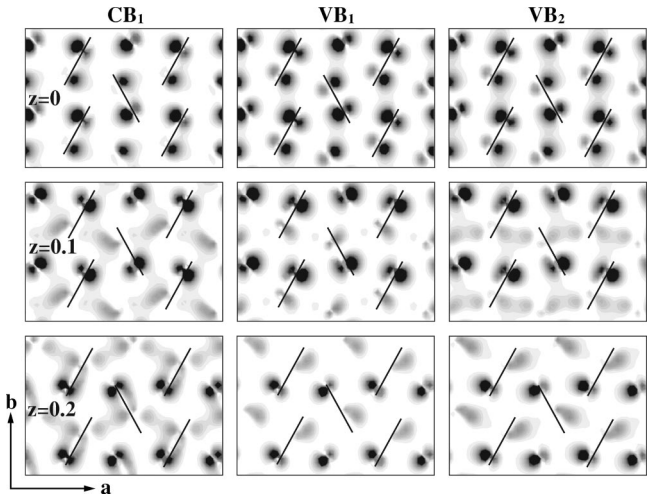

FIG. 6. 2D-electron density plots of CB_1, VB_1, and VB_2 in the (ab) plane calculated as sum over 40 $\boldsymbol{k}$ points along $\overline{\Gamma KZ}$ at ambient pressure for different z coordinates in units of c. The solid lines indicate the molecules to illustrate the herringbone arrangement. The dark regions correspond to high density and vice versa.

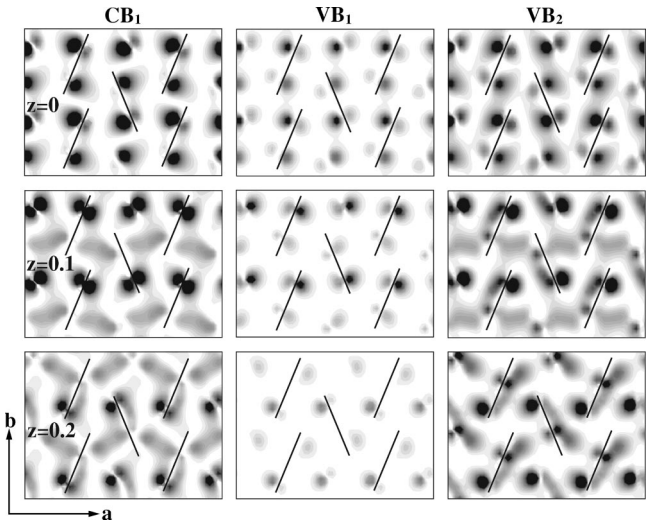

FIG. 7. 2D-electron density plots of CB_1, VB_1, and VB_2 in the (ab) plane calculated as sum over 40 $\boldsymbol{k}$ points along along $\overline{\Gamma KZ}$ at 10.2 GPa for different z coordinates in units of c. The solid lines indicate the molecules to illustrate the herringbone arrangement. The dark regions correspond to high density and vice versa.

with pressure. The *bonding* states (CB_1 and VB_2) significantly raise the π-electron density in the interstitial region, which is in contrast to the *antibonding* band VB_1. While they are rather similar at ambient pressure, VB_1 exhibits highly diminished electron density between neighboring molecules at 10.2 GPa compared to its *bonding* counterpart VB_2 leading to its localized behavior. This explains the decrease in dispersion of VB_1 in contrast to the increase of VB_2 in this part of the band structure. Another interesting feature is the electron distribution in the interstitial. We suppose that the herringbone arrangement of the molecules favors the maximum overlap of the π-wave functions. With increasing pressure the molecules orient in such a way that this overlap can be sustained. Similar results have been obtained for biphenyl.[31,32]

E. Energy gap and optical properties

The previously described pressure effects reduce the band gap E_g of anthracene. At ambient pressure the LDA gap is 2 eV, which is underestimated compared to the true energy gap. In order to be consistent with the experimental value of 3.9 eV,[23] we have taken into account a self-energy correction Δ_c of 1.9 eV. As a consequence of the energy gap reduction and increase of the bandwidths we obtain a redshift and a broadening of the optical absorption peaks, respectively. In Fig. 8 the y component (top panel) and z component (bottom panel) of the imaginary part of the dielectric tensor as a function of pressure are presented. Apart from the x component, there is also a small off-diagonal xz component present according to the monoclinic symmetry. Both are small compared to the main components and therefore not included in Fig. 8. We obtain a weak y-polarized transition at the band-gap edge and a strong z-polarized peak next in energy. The y-polarized (z-polarized) transition describes the optical absorption with the electric field vector of the probing light

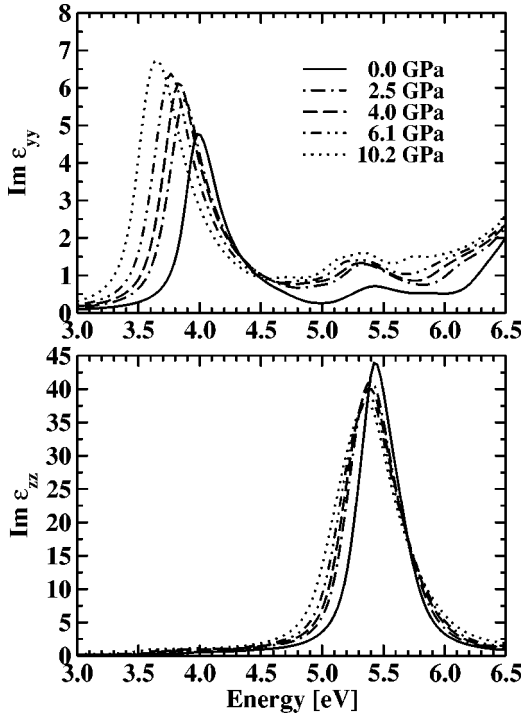

FIG. 8. Imaginary part of the dielectric tensor computed at several pressure values up to 10.2 GPa separated in *y*-polarized (top panel) and *z*-polarized components (bottom panel). The spectra are rigidly shifted by a Δ_c of 1.9 eV and a lifetime broadening of 0.1 eV has been included.

parallel to the short (long) molecular axis. Without the self-energy correction these transitions appear at 2 and 3.5 eV at ambient pressure and are corrected to 3.9 and 5.4 eV when including Δ_c. Assuming a pressure independent scissors operator we can determine the average gap reduction and redshift of the lowest optical transition. In Fig. 9 we plot the band gap E_g and the peak position of the lowest optical absorption as a function of pressure. According to the non-uniform pressure dependence of the structural properties, both the energy gap reduction and the redshift of the *y*-polarized optical absorption are more strongly pronounced in the low-pressure range compared to the high-pressure region. When applying a linear fit to the lower and upper pressure range, respectively, the average decrease of E_g up to 3 GPa is -0.1 eV/GPa and -0.04 eV/GPa from 3 to 10.2 GPa. Analogously, the redshift of the *y*-polarized (*z*-polarized) absorption peak is -0.053 eV/GPa (-0.009 eV/GPa), whereas it is reduced to -0.023 eV/GPa (-0.004 eV/GPa) for higher pressures. These data agree well with early measurements of the near-ultraviolet and visible absorption peaks of anthracene by Wiederhorn and Drickamer,[33] which confirm the redshift and the broadening as a function of pressure. They observe a linear redshift of approximately -0.06 eV/GPa for the lowest absorption peak, which is constant up to 5 GPa. In the higher pressure region the redshift is diminished and nonlinear. Although our theoretical findings reproduce the general experimental trend, additional polarized optical absorption spectra under well defined pressure conditions would be highly appreciated for a detailed quantitative comparison between theory and experiment.

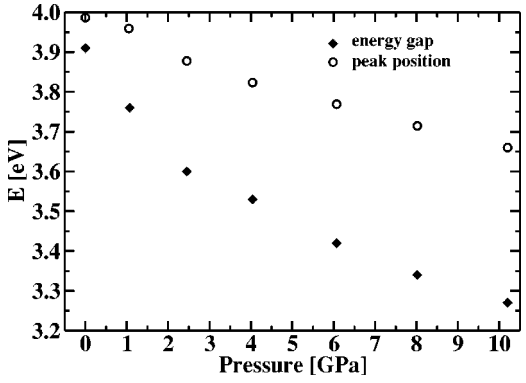

FIG. 9. The band gap E_g (diamonds) and the peak position of the *y*-polarized lowest optical absorption (open dots) as a function of pressure. A self-energy Δ_c of 1.9 eV has been included.

IV. DISCUSSION AND CONCLUSIONS

In this study we faced one of the major problems of LDA, the well-known overbinding effect,[34] which is responsible for the underestimation of the equilibrium volume and the overestimation of the bulk modulus. In particular, it has been argued that the strength of the hydrogen bond is seriously overestimated in LDA,[35] but the gradient corrected functionals (GGA's) successfully compensate for this effect.[18,36,37] However, both types of functionals have shortcomings in the description of weak long-range interactions such as the vdW force.[35,36,38–40] In Ref. 37 the equilibrium bond lengths, atomization energies, and vibrational frequencies of a variety of rare-gas dimers from DFT calculations utilizing three xc functionals, the LDA-PW91,[41] the GGA-PW91,[42] and the GGA-PBE[18] are reported. This study allows to conclude that GGA functionals significantly improve the LDA values. Moreover, they found that the GGA-PBE functional leads to bound dimers. In contrast, a similar study of a benzene dimer and orthorhombic benzene using LDA and GGA functionals[35] revealed that the GGA's give a mechanically unstable crystal. Therefore it could be argued that the well-known overbinding of the LDA potential compensates for the missing vdW force and for that reason leads to reasonable results concerning the internal geometry. In analogy to benzene and the rare-gas dimers, it is commonly believed that the vdW interaction is the main bonding force in organic molecular crystals. Therefore we want to discuss wether the application of LDA and GGA for the description of anthracene is valid. LDA and GGA yield similar internal structure parameters. This gives rise to the conclusion that the internal geometry does not significantly depend on the xc potential used. Since the theoretical results are reproduced by the Rietveld refinement of experimental data (Fig. 2), we further conclude that LDA, as well as GGA, are able to correctly describe the internal structure of organic molecular crystals. Therefore the reliability of such methods within DFT for these investigations is confirmed. On the other hand, if the vdW forces were the *glue* between neighboring molecules

and LDA compensated for this interaction, we would expect that GGA does not give a stable crystal at all. For this reason we analyzed the LDA and GGA total energies as a function of the unit-cell volume. LDA predicts the theoretical equilibrium volume V_{LDA} at 422 Å^3, which is 11% smaller than the experimental volume at ambient pressure V_{exp}. In contrast, a parabolic fit of the GGA total energies corresponding to the contracted structures suggests an equilibrium structure with a volume larger than V_{exp}, which needs to be verified. For this purpose the lattice parameters and the three angles specifying the internal geometry have been extrapolated in order to obtain good starting geometries for the expanded structures with unit-cell volumes increased by 4, 7, 14, and 24%, respectively. The structure optimization has followed the same procedure as explained in Sec. II A. The so obtained optimized internal geometry reasonably follows the trend of the extrapolation of the pressure data. From this procedure one can conclude that GGA is also able to yield a bound crystal, but with an equilibrium volume 16% larger than the experimental one. However, since the values corresponding to the expanded volumes rely on the assumption that such an extrapolation is valid and also slightly deviate from a parabolic fit, they are not completely convincing. For this reason we analyzed the electron density calculated with GGA. The results reproduce the LDA findings, i.e., significant density contributions between the molecules. These findings give strong evidence that the vdW interaction is not solely the driving force for the bonding mechanism in anthracene.

ACKNOWLEDGMENTS

This work was supported by the Austrian Science Fund (projects 14237-PHY and 14004-PHY) and by the EU research and training network *EXCITING*, contract number HPRN-CT-2002-00317. P.P. acknowledges a grant from the Austrian Academy of Sciences.

*Author to whom correspondence should be addressed. kerstin.hummer@uni-graz.at; homepage: http://physik.uni-graz.at/~kew/

[1] H. Shirakawa, E. J. Louis, A. G. MacDiarmid, C. K. Chiang, and A. J. Heeger, J. Chem. Soc. Chem. Commun. **1977**, 578.
[2] C. K. Chiang, C. R. Fincher, Y. W. Park, A. J. Heeger, H. Shirakawa, E. J. Louis, S. C. Gau, and A. G. MacDiarmid, Phys. Rev. Lett. **39**, 1098 (1977).
[3] P. W. M. Blom and M. C. J. M. Vissenberg, Mater. Sci. Eng., B **27**, 53 (2000).
[4] D. Kim, H. Cho, and C. Y. Kim, Prog. Polym. Sci. **25**, 1089 (2000).
[5] C. Hosokawa, H. Higashi, and T. Kusumoto, Appl. Phys. Lett. **62**, 3238 (1993).
[6] L. Torsi, A. Dodabalapur, L. J. Rothberg, A. W. P. Fung, and H. E. Katz, Science **272**, 1462 (1996).
[7] W. Waragai, H. Akimichi, S. Hotta, H. Kano, and H. Sakaki, Phys. Rev. B **52**, 1786 (1995).
[8] O. H. L. Blanc, J. Chem. Phys. **33**, 626 (1960).
[9] N. Karl and J. Marktanner, Mol. Cryst. Liq. Cryst. Sci. Technol., Sect. A **355**, 149 (2001).
[10] M. E. Hamamsy and A. C. D. S. A. Elnahwy, Mol. Cryst. Liq. Cryst. **95**, 209 (1983).
[11] R. M. Glaeser and R. S. Berry, J. Chem. Phys. **44**, 3797 (1966).
[12] L. B. Schein, C. B. Duke, and A. R. McGhie, Phys. Rev. Lett. **40**, 197 (1978).
[13] R. Mason, Acta Crystallogr. **17**, 547 (1964).
[14] P. Blaha, K. Schwarz, and J. Luitz, *WIEN97, A Full Potential Linearized Augmented Plane Wave Package or Calculating Crystal Properties* (Karlheinz Schwarz, Technische Universität Wien, Vienna, 1999), ISBN 3–9501031–0–4.
[15] M. Oehzelt, R. Resel, and A. Nakayama, Phys. Rev. B **66**, 174104 (2002).
[16] E. Sjöstedt, L. Nordström, and D. J. Singh, Solid State Commun. **114**, 15 (2000).
[17] D. M. Ceperley and B. J. Alder, Phys. Rev. Lett. **45**, 566 (1980).
[18] J. P. Perdew, K. Burke, and M. Ernzerhof, Phys. Rev. Lett. **77**, 3865 (1996).
[19] P. E. Blöchl, O. Jepsen, and O. K. Andersen, Phys. Rev. B **49**, 16 223 (1994).
[20] H. Ehrenreich and M. H. Cohen, Phys. Rev. **115**, 786 (1959).
[21] R. DelSole and R. Girlanda, Phys. Rev. B **48**, 11 789 (1993).
[22] M. S. Hybertsen and S. G. Louie, Phys. Rev. B **34**, 5390 (1986).
[23] E. A. Silinsh, *Organic Molecular Crystals* (Springer-Verlag, Berlin, 1980), ISBN 3-540-10053-9.
[24] F. Birch, J. Geophys. Res. **83**, 1257 (1978).
[25] M. Oehzelt, G. Heimel, R. Resel, P. Puschnig, K. Hummer, C. Ambrosch-Draxl, and A. Nakayama (unpublished).
[26] W. Häfner and W. Kiefer, J. Chem. Phys. **86**, 4582 (1987).
[27] A. S. Davydov, *Theory of Molecular Excitons* (Plenum Press, New York, 1971).
[28] J. L. Katz, S. A. Rice, S.-I. Choi, and J. Jortner, J. Chem. Phys. **39**, 1683 (1963).
[29] R. Silbey, J. Jortner, S. A. Rice, and M. T. Vala, J. Chem. Phys. **42**, 733 (1965).
[30] R. Silbey, J. Jortner, S. A. Rice, and M. T. Vala, J. Chem. Phys. **43**, 2925 (1965).
[31] P. Puschnig, *Excitonic Effects In Organic Semi-Conductors* (Shaker-Verlag, Aachen, Germany, 2002), ISBN 8-8322-0098-3.
[32] P. Puschnig, K. Hummer, and C. Ambrosch-Draxl (unpublished).
[33] S. Wiederhorn and H. G. Drickamer, J. Phys. Chem. Solids **9**, 330 (1959).
[34] A. van de Walle and G. Ceder, Phys. Rev. B **59**, 14 992 (1999).
[35] E. J. Meijer and M. Sprik, J. Chem. Phys. **105**, 8684 (1996).
[36] P. Zische, S. Kurth, and J. P. Perdew, Comput. Mater. Sci. **11**, 122 (1998).
[37] D. C. Patton and M. R. Pederson, Phys. Rev. A **56**, R2495 (1997).
[38] N. Kurita and H. Sekino, Chem. Phys. Lett. **348**, 139 (2001).
[39] E. Hult, Y. Andersson, B. I. Lundqvist, and D. C. Langreth, Phys. Rev. Lett. **77**, 2029 (1996).
[40] R. Hult, H. Rydberg, B. I. Lundqvist, and D. C. Langreth, cond-mat/9805352 (unpublished).
[41] J. P. Perdew and Y. Wang, Phys. Rev. B **45**, 13 244 (1992).
[42] J. P. Perdew, J. A. Chevary, S. H. Vosko, K. A. Jackson, M. R. Pederson, D. J. Singh, and C. Fiolhais, Phys. Rev. B **46**, 6671 (1992).